Critical thickness investigation of magnetic properties in exchange-coupled bilayers

R. L. Rodríguez-Suárez,[1] L. H. Vilela-Leão,[2] T. Bueno,[2] A. B. Oliveira,[3,4] J. R. L. de Almeida,[2]
P. Landeros,[5] S. M. Rezende,[2] and A. Azevedo[2]

[1]*Facultad de Física, Pontificia Universidad Católica de Chile, Casilla 306, Santiago, Chile*
[2]*Departamento de Física, Universidade Federal de Pernambuco, Recife, PE 50670-901, Brazil*
[3]*Departamento de Física Teórica e Experimental, Universidade Federal do Rio Grande do Norte, 59078-970 Natal, RN, Brazil*
[4]*Escola de Ciências e Tecnologia, Universidade Federal do Rio Grande do Norte, 59078-970, Natal, RN, Brazil*
[5]*Departamento de Física, Universidad Técnica Federico Santa María, Avenida España 1680, 2390123 Valparaíso, Chile*

(Received 7 December 2010; revised manuscript received 30 March 2011; published 24 June 2011)

We present a systematic investigation of the magnetic properties of two series of polycrystalline ferromagnetic-antiferromagnetic bilayers (FM-AF) of $Ni_{81}Fe_{19}(10nm)/Ir_{20}Mn_{80}(t_{AF})$ grown by dc magnetron sputtering. One series was grown at an oblique angle of 50° and the other one was grown at 0°. Ferromagnetic resonance (FMR) was used to measure the exchange bias field H_E, the rotatable anisotropy field H_{RA}, and the FMR linewidth ΔH as a function of the antiferromagnetic layer thickness t_{AF}. Three relaxation channels due to isotropic Gilbert damping, anisotropic two-magnon scattering, and mosaicity effects are simultaneously distinguished through the angular dependence of the FMR linewidth. In the regime of small IrMn layer thicknesses, not enough to establish the exchange bias anisotropy, the FMR linewidth shows a sharp peak due to the contribution of the two-magnon scattering mechanism. The results presented here are of general importance for understanding the dynamics of magnetization in the FM-AF structures.

DOI: 10.1103/PhysRevB.83.224418 PACS number(s): 75.70.Cn, 76.50.+g, 75.30.Et

I. INTRODUCTION

Since the discovery in 1956 by Meiklejohn and Bean[1] of the exchange bias (EB) phenomenon, a complete theoretical understanding of the magnetic coupling phenomena between a ferromagnetic (FM) and an antiferromagnetic (AF) material has posed one of the most remarkable challenges in the field of magnetism. While the phenomenon is observed in a large variety of systems,[2–4] it is in thin-film multilayers that it has found important technological applications, as a domain stabilizer of magnetoresistive heads and in spin valve design. Complete references can be found in some recent reviews published on this subject.[2–8]

Despite the large amount of research reported on the topic, there are still several aspects of the EB mechanism at the FM-AF interface that are not well understood. For instance, the complete origin of rotatable anisotropy and the fact that different measurement techniques may yield different values for the FM-AF exchange field (H_E) between the layers still lack a satisfactory elucidation.[9,10] In addition, the mechanism that controls the spin structure at the interface is still controversy. Néel[11] was the first one to realize that FM-AF coupling involves so many aspects to be well explained by a simple model such as the one initially proposed by Meiklejohn and Bean[1] from which the values of H_E predicted are typically two orders of magnitude larger than the experimental results. In order to predict reasonable values for H_E, Mauri *et al.*[12] proposed the first domain-wall model of EB. Although this model results in more reasonable values for H_E, it cannot explain features such as the enhanced coercivity H_C of the FM-AF bilayer systems, or the training effect.

A model proposed by Stiles and McMichael[13] to describe the behavior of polycrystalline FM-AF bilayers is based on the existence of independent AF grains that are coupled to the FM film at the FM-AF interface. Some of the grains are large enough in order to stabilize the AF order and therefore are responsible for the existence of uniaxial anisotropy. On the other hand, the smaller grains, in which the AF magnetization rotates irreversibly as the FM magnetization rotates, are responsible for hysteretic behavior observed in torque curve measurements and for the overall shift of the resonance field observed in ferromagnetic resonance (FMR) measurements. These irreversible transitions set the system to lower-energy states, meaning that, on average, the easy direction of these grains goes along with the FM magnetization direction. This behavior is phenomenologically described by a rotatable field that always points along the local FM magnetization vector. This model has been successfully used to explain most of the properties measured by both FMR and dc magnetization techniques in FM-AF bilayers.

Many experimental results have shown that the exchange field H_E and coercivity H_C in FM-AF bilayers are inversely proportional to the FM layer thickness.[14] On the other hand, the dependence of the magnetic properties on the AF layer thickness needs a much more elaborate analysis. For instance, there exists a critical thickness of the AF below which the EB vanishes.[15,16] In addition to this, it has been observed that the coercivity and the rotatable anisotropy field show maximum values for different AF layer thicknesses.[15, 17–21]

FM resonance has been shown to be one of the most successful techniques used to determine the values of the effective fields associated with the magnetic anisotropies in FM thin films and multilayers.[22–26] In addition, FMR linewidth measurements also give accurate information about the magnetic relaxation mechanisms in these systems. Because they are very sensitive to the details of microscopic interactions and materials microstructure, the FMR linewidths can give relevant information about the magnetization dynamics of FM-AF systems. It also provides powerful insight into the nature of the FM-AF interactions that cannot be obtained by other techniques.

In this paper we present a systematic investigation of magnetic properties in polycrystalline FM-AF bilayers as a function of the AF layer thickness. The angular dependences of the FMR resonance field and linewidth are analyzed by the Landau-Lifshitz-Gilbert (LLG) equation. It is found that the in-plane angular dependence of the FMR linewidths can be described by a superposition of different mechanisms, such as the intrinsic Gilbert damping effect, magnetic inhomogeneity, and two-magnon scattering. By investigating the in-plane dependence of the FMR linewidth for a series of Py(10 nm)/IrMn(t_{AF}), we are able to separate the contribution of the different relaxation mechanisms to the magnetization damping. For instance, in the low t_{AF} regime (below the EB onset), the rise in ΔH is mainly associated with the presence of the two-magnon scattering process. The analysis carried out in this work is certainly relevant for understanding the magnetization dynamics in EB polycrystalline thin films.

II. EXPERIMENT

The samples investigated here are multilayers of Cu(6 nm)/$Ni_{81}Fe_{19}$(10 nm)/$Ir_{20}Mn_{80}$(0–16.4 nm) (labeled series A) and Cu(6 nm)/$Ni_{81}Fe_{19}$(10 nm)/$Ir_{20}Mn_{80}$(0–6.1 nm) (labeled series B). Series B was grown by sputter deposition at an oblique angle 50° and series A was grown at 0°. The films were deposited by dc magnetron sputtering system on commercially available Si(001) after being cleaned in ultrasound baths of acetone and ethanol for 30 min and dried in nitrogen flow. The base pressure was 2.2×10^{-7} Torr. In order to establish the uniaxial anisotropy of the FM layer, a magnetic field of ∼50 Oe was applied on the sample surface during deposition.

The FMR data were taken with a homemade *X*-band spectrometer operating at 8.61 GHz, with the sample mounted on the tip of an external goniometer and introduced through a hole in the back wall of the cavity. Thus, it could be rotated to allow measurements of the in-plane resonance field H_R and linewidth ΔH as a function of the azimuthal angle, which were determined by fitting the derivative of a Lorentzian line shape to the measured field spectrum and the peak-to-peak field spacing, respectively. The dc magnetic field was provided by a 9-in. electromagnet and was modulated with a 1.2-kHz ac component of a few Oersteds using a pair of Helmholtz coils to allow lock-in detection of the absorption derivative.

III. THEORETICAL BACKGROUND

The magnetization dynamics in the FM layer can be described by the LLG equation[27,28]

$$\frac{d\mathbf{M}_{FM}}{dt} = -\gamma \mathbf{M}_{FM} \times \mathbf{H}_{eff} + \alpha \left(\mathbf{M}_{FM} \times \frac{\partial \hat{\mathbf{m}}}{\partial t} \right), \qquad (1)$$

where γ is the absolute value of the electron gyromagnetic ratio, $\hat{\mathbf{m}}$ is the unit vector in the direction of the FM magnetization vector $\mathbf{M}_{FM}$, and α is the dimensionless Gilbert damping parameter. The first term in Eq. (1) represents the precessional torque in the effective magnetic field $\mathbf{H}_{eff}$ and the second term represents the well-known Gilbert damping torque.[28]

Considering only the first term in Eq. (1) and following the Smit and Beljers scheme,[29] the dispersion relation for the FM-AF bilayer can be calculated from the roots of a 4×4 matrix.[30] Then, the resonance condition obtained is

$$\left(\frac{\omega^2}{\gamma^2}\right) = \left[\left(E_{\phi_{FM}\phi_{FM}} - \frac{E^2_{\phi_{FM}\phi_{AF}}}{E_{\phi_{AF}\phi_{AF}}}\right)\left(E_{\theta_{FM}\theta_{FM}} - \frac{E^2_{\theta_{FM}\theta_{AF}}}{E_{\theta_{AF}\theta_{AF}}}\right)\right] \times \frac{1}{(t_{FM}M_{FM})^2}, \qquad (2)$$

where t_{FM} is the FM layer thickness and each term E_{ij} denotes the second derivative of the free energy per unit surface with respect to the equilibrium angles of the ferromagnetic (ϕ_{FM}) and the antiferromagnetic (ϕ_{AF}) magnetization. In deriving Eq. (2), we consider that the dc magnetic field is applied in the plane of the sample, therefore, we can regard that the magnetizations of the both layers are in the plane, i.e., $\theta_{FM} = \theta_{AF} = \pi/2$.

The behavior of the system can be described by a phenomenological model in terms of the magnetic free energy. Here we assume that a magnetization domain wall sets up at the AF layer as the FM magnetization rotates away from the equilibrium position. In the framework of this model, the magnetic free energy per unit area of the FM-AF bilayer can be written as

$$E = \left[-\mathbf{H}\cdot\mathbf{M}_{FM} + \left(2\pi M^2_{FM} - \frac{K_S}{t_{FM}}\right)\left(\frac{\mathbf{M}_{FM}\cdot\hat{\mathbf{n}}}{M_{FM}}\right)^2 - K_U\left(\frac{\mathbf{M}_{FM}\cdot\hat{\mathbf{u}}_{FM}}{M_{FM}}\right)^2\right] t_{FM} - J_E\frac{\mathbf{M}_{FM}\cdot\mathbf{M}_{AF}}{M_{FM}M_{AF}} - \sigma_W\frac{\mathbf{M}_{AF}\cdot\hat{\mathbf{u}}_{AF}}{M_{AF}} - (\mathbf{M}_{FM}\cdot\mathbf{H}_{RA})\, t_{FM}, \qquad (3)$$

where the first three terms in order are the Zeeman, demagnetizing, and uniaxial anisotropy energies of the FM layer, with K_S and K_U the surface and uniaxial anisotropy constants, respectively. The fourth and fifth terms are the FM-AF exchange coupling and the AF domain-wall energies, respectively. The last term in Eq. (3) is the rotatable anisotropy energy,[13] where H_{RA} is the corresponding effective field which accounts for the spins at the AF part of the FM-AF interface that rotate together with the FM magnetization. The unit vectors $\hat{\mathbf{n}}$, $\hat{\mathbf{u}}_{FM}$, and $\hat{\mathbf{u}}_{AF}$ represent the normal to the film's surface direction, the FM uniaxial anisotropy direction, and the AF pinning direction, respectively. Figure 1 shows the coordinate system used to describe these vectors and the orientation of the magnetizations $\mathbf{M}_{FM}$, $\mathbf{M}_{AF}$, as well as the applied magnetic field $\mathbf{H}$ direction.

For the resonance field values measured in this work, the magnetization and the external field are parallel, i.e., $\phi_{FM} \cong \phi_H$ and from Eqs. (2) and (3) the FMR frequency is given by

$$\omega = \gamma\sqrt{H_Y H_Z}, \qquad (4)$$

where

$$H_Y = H + H_U\cos 2(\phi_H - \eta) + H_{RA} + H_2^{eff} \qquad (5)$$

and

$$H_Z = H + 4\pi M_{eff} + H_U\cos^2(\phi_H - \eta) + H_{RA} + H_1^{eff}, \qquad (6)$$

where[24]

$$H_1^{\text{eff}} = \frac{H_W \cos\phi_{\text{AF}} \cos(\phi_{\text{H}} - \phi_{\text{AF}} - \beta) - H_E \sin^2(\phi_{\text{H}} - \phi_{\text{AF}} - \beta)}{\frac{H_W}{H_E} \cos\phi_{\text{AF}} + \cos(\phi_{\text{H}} - \phi_{\text{AF}} - \beta)} \tag{7}$$

and

$$H_2^{\text{eff}} = \frac{H_W \cos\phi_{\text{AF}} \cos(\phi_{\text{H}} - \phi_{\text{AF}} - \beta)}{\frac{H_W}{H_E} \cos\phi_{\text{AF}} + \cos(\phi_{\text{H}} - \phi_{\text{AF}} - \beta)}. \tag{8}$$

Here, H is the strength of applied magnetic field, $H_U = 2K_U/M_{\text{FM}}$ is the FM uniaxial anisotropy field, $H_E = J_E/(t_{\text{FM}} M_{\text{FM}})$ is the exchange coupling field, $H_W = \sigma_W/(t_{\text{FM}} M_{\text{FM}})$ is the domain-wall effective field, and M_{eff} is the effective magnetization defined by $4\pi M_{\text{eff}} = 4\pi M_{\text{FM}} - H_S$, where $H_S = 2K_S/M_{\text{FM}} t_{\text{FM}}$ is the surface anisotropy field. As shown in Fig. 1, the easy axes of both FM and AF layers are supposed to be oriented along the angles η and β respectively, with respect to the reference direction that is the direction of the applied magnetic field during the growth.

From Eq. (4), we can write the resonance field H_R as function of the azimuthal angle ϕ_H as

$$H_R = \frac{1}{2}\Bigg[H_U(1 - 3\cos^2(\phi_H - \eta)) - 4\pi M_{\text{eff}} - 2H_{\text{RA}} - H_1^{\text{eff}} - H_2^{\text{eff}} + \sqrt{\left[H_U \sin^2(\phi_H - \eta) + 4\pi M_{\text{eff}} + H_1^{\text{eff}} - H_2^{\text{eff}}\right]^2 + 4\left(\frac{\omega}{\gamma}\right)^2}\Bigg]. \tag{9}$$

Thus we can determine the anisotropy fields from the measured angular dependence of H_R. As we pointed out, the second term in Eq. (1) corresponds to the phenomenological Gilbert damping torque, which leads to a finite width of the resonance signal in a FMR experiment. However, not all the magnetization damping processes can be written as the Gilbert damping term. We have to add the so-called extrinsic relaxation processes, and their quantitative description depends on the specific physical origin of the phenomenon responsible by the energy loss.

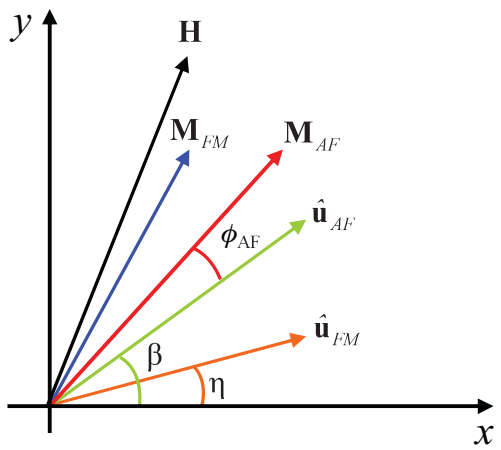

FIG. 1. (Color online) Coordinate system used in the ferromagnetic resonance analysis. All the vectors are in the film plane (xy plane).

In this work, the measured FMR linewidths are analyzed taking into consideration the superposition of three different contributions,

$$\Delta H = \Delta H_{\text{Gilbert}} + \Delta H_{2M} + \Delta H^{\text{mosaic}}, \tag{10}$$

where ΔH denotes the peak-to-peak linewidth of the FMR signal. Here, the first term corresponds to the standard Gilbert contribution, which is derived directly from the LLG equation (1), leading to the linewidth given by[31]

$$\Delta H_{\text{Gilbert}} = \frac{2}{\sqrt{3}} \frac{\alpha}{\gamma} \omega. \tag{11}$$

The second term in Eq. (10) is the two-magnon contribution to the linewidth, ΔH_{2M}, which is caused by scattering of the uniform ($\mathbf{k} = \mathbf{0}$) precession mode, excited by FMR, into nonuniform modes ($\mathbf{k} \neq \mathbf{0}$ magnons) that are degenerate in frequency.[32–39] As such a process cannot conserve momentum, it requires the presence of defects that serve as scatterers in order to conserve the total momentum. To describe the two-magnon contribution to the FMR linewidth in our films, we use the Arias-Mills formulation,[32–39] in which the angular dependence of the linewidth ΔH_{2M} is obtained by introducing a scattering matrix of extrinsic nature into the spin-wave Hamiltonian, leading to

$$\Delta H_{2M} = \frac{\Gamma_0}{(H_Y + H_Z)^2}\Bigg\{H_Y^2 + [H_Y \cos^2\phi_H + H_Z \cos(2\phi_H)]^2 \times \left(\left\langle\frac{a}{c}\right\rangle - 1\right) + [H_Y \sin^2\phi_H - H_Z \cos(2\phi_H)]^2 \times \left(\left\langle\frac{c}{a}\right\rangle - 1\right)\Bigg\} \sin^{-1}\sqrt{\frac{H_Y}{H_Z}}. \tag{12}$$

In this formulation, the surface and interface roughness of the films occurring on the short length scales results in a variation of the surface anisotropy that can activate two-magnon scattering. Here, the defects are supposed to be rectangular in shape, with height b and lateral dimensions a and c randomly distributed. It is important to note that Eq. (12) is a generalization of Eq. (94) of Ref. 33, in which we include the in-plane uniaxial anisotropy for the case where the external field **H** is applied, making an angle ϕ_H with the easy axis.[40]

The last term in Eq. (10) is the line broadening due to the mosaicity (ΔH^{mosaic}). This term is caused by a small spread of parameters on a very large scale.[37,41,42] The simplest model of the FMR linewidth and inhomogeneity attributes the inhomogeneous broadening to parameter variations within the sample. This variation can be found in the internal fields, magnetization, surface anisotropy, film thickness, and magnetocrystalline anisotropy. Thus, individual regions of the film will have slightly different resonance fields. Here, we will consider fluctuations in the uniaxial anisotropy field directions and in the exchange coupling field strength H_E. Then, the resulting spread of resonance frequencies yields a field linewidth that is given by[37,41,42]

$$\Delta H^{\text{mosaic}} = \left|\frac{\partial H_R}{\partial \eta}\Delta\eta\right| + \left|\frac{\partial H_R}{\partial \beta}\Delta\beta\right| + \left|\frac{\partial H_R}{\partial H_E}\Delta H_E\right|, \quad (13)$$

where $\Delta\eta$ and $\Delta\beta$ represent the average spread of the direction of the easy axes of the FM and the AF films, respectively, and ΔH_E represents the strength variation of H_E at the FM-AF interface.

IV. RESULTS AND DISCUSSION

In this section we present the experimental results and interpretation, including a comparison with the theoretical results. The effective magnetization value $4\pi M_{\text{eff}} = 9.93$ kG was extracted from the fit of the experimental data corresponding to the $Ni_{81}Fe_{19}$ film, where $\gamma = 17.6$ GHz/kOe. Figure 2 shows the in-plane dependence of the FMR field for three bilayers of $Ni_{81}Fe_{19}$(10 nm)/$Ir_{20}Mn_{80}$(t_{AF}) of series A with t_{AF}=1.2, 4.2, and 12 nm. The solid line in each case corresponds to the best fit to the experimental data using Eq. (9) from which the values of the exchange and anisotropy fields were extracted. Notice that when the AF thickness increases, the average value of the resonance field is overall downshifted by an amount that corresponds to the rotatable anisotropy field H_{RA}, as seen in Eq. (9). At small t_{AF}, the curves exhibit the symmetry of a typical uniaxial anisotropy, and for large t_{AF} the curves show a bell-shaped symmetry, which is typical of unidirectional anisotropy as expected for the case in which $H_E \gg H_U$.

Figure 3(a) shows the behavior of the EB field H_E (circles) and the rotatable anisotropy field H_{RA} (squares) as a function of the $Ir_{20}Mn_{80}$ layer thickness t_{AF} for samples of series A. Three regions are clearly distinguished, shown in Fig. 3(a) as separated by vertical dashed lines: In region I, where the AF layer thickness is smaller than the critical thickness, $t_{\text{AF}} < t_{\text{cr}} = 40$ Å, the EB H_E field vanishes, and the H_{RA} field increases sharply with increasing thickness; region II, with 40 Å $< t_{\text{AF}} <$ 80 Å, where the EB reaches the saturation value and the rotatable anisotropy field reduces monotonically with

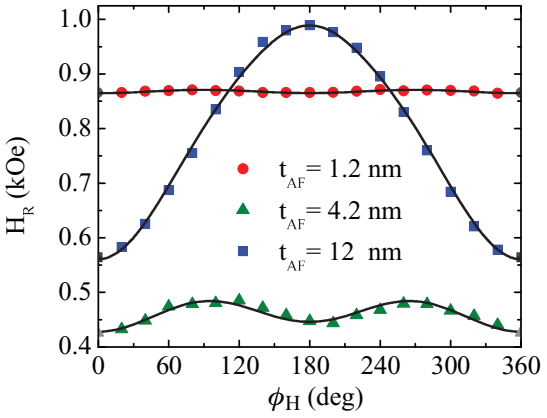

FIG. 2. (Color online) In-plane angular dependence of the FMR field for a series of NiFe/IrMn bilayers grown at a deposition angle of 0°. While the FM layer thickness is fixed in 10 nm, we show data for three different AF layer thicknesses t_{AF}=1.2, 4.2, and 12 nm.

an increasing thickness value; and region III for $t_{\text{AF}} > 80$ Å, where both H_E and H_{RA} reach their saturation values. In region I the increase in H_{RA} is attributed to the establishment of the AF order of the $Ir_{20}Mn_{80}$ layer. However, since $H_E = 0$ in this region, the AF order occurs in the rotatable AF grain regime.[13] At $t_{\text{AF}} \cong 40$ Å, where the EB anisotropy starts to establish, H_{RA} reaches its maximum value. In region II, opposite trends for H_E and H_{RA} indicate that changes at the FM-AF interface occur,[15] with the increase of H_E produced by the increasing number of the stable AF grains at the expense of a reduction in the number of the rotatable ones. In region III, for $t_{\text{AF}} > 80$ Å, both H_E and H_{RA} attain their saturation values because most of the IrMn grains at the interface are magnetically stable.

The FMR linewidth dependence as a function of the AF layer thickness, for the samples of series A, is consistent with the analysis discussed above. With the increase of the AF layer

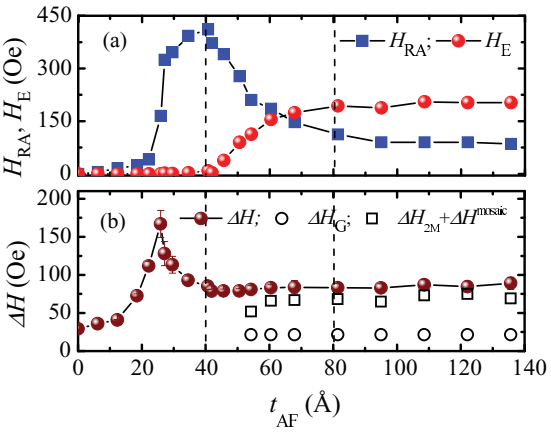

FIG. 3. (Color online) (a) AF layer thickness dependence of the EB field H_E (circles) and rotatable anisotropy field H_{RA} (squares) obtained from the fitting of the FMR data. (b) AF layer thickness dependence of the FMR linewidth (circles). The linewidth value is averaged over all the in-plane resonance spectra for each sample. The FM-AF bilayers were grown at a deposition angle of 0°. The solid lines in (a) and (b) are guides for the eyes.

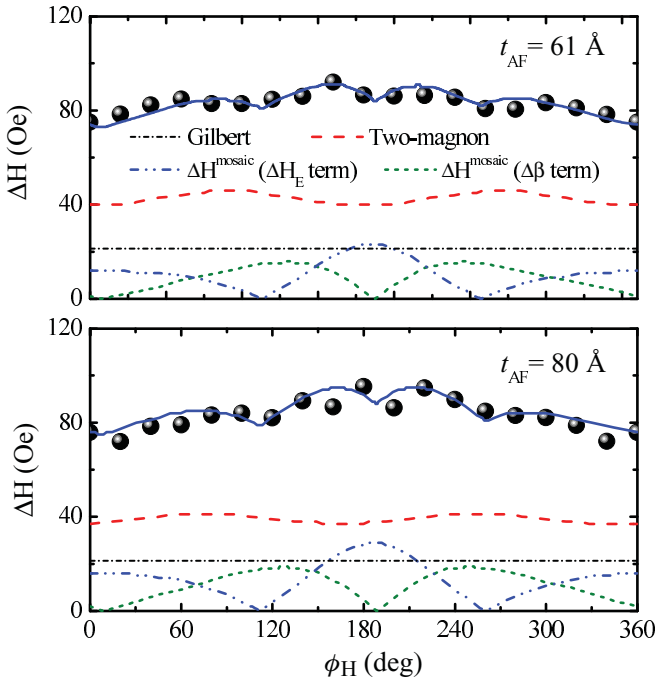

FIG. 4. (Color online) Angular dependence of the FMR linewidth for the bilayers deposited at an angle of 0°. The circles are the experimental data obtained at a frequency of 8.61 GHz, whereas the solid lines are fits obtained from Eq. (10) with the parameters showed in Table I. The dashed lines correspond to the individual contributions of the three relaxation mechanisms considered.

thickness, ΔH initially increases, exhibiting a peak value at $t_{AF} \cong 26$ Å, and then decreases until it reaches a saturation value at $t_{AF} \cong 42$ Å. Notice that the abrupt variation of ΔH occurs in region I, where H_{RA} also varies sharply and the EB field vanishes. Hence, both behaviors are mostly related to the same interface phenomenon. In fact, the existence of AF grains at the interface can contribute to the enhancement of the magnetic damping with two different mechanisms: two-magnon scattering and mosaicity, as described in Sec. III. In order to determine the contributions from the two relaxation mechanisms, we have investigated the angular dependence of the FMR linewidth.

Figure 4 shows the linewidth data (symbols) and theoretical fits (solid lines) obtained with the model based on Eq. (10) for two different Py(10 nm)/IrMn(t_{AF}) bilayers of series A, with $t_{AF} = 61$ and 80 Å. The parameters used to fit the angular dependence of the FMR linewidth are the Gilbert damping coefficient α of Eq. (11), Γ_0 and $\langle c/a \rangle$ of the expression corresponding to the two-magnon contribution [Eq. (12)], as well as $\Delta\eta$, $\Delta\beta$, and ΔH_E of Eq. (13) (see Table I). The values of $4\pi M_{eff}$ and the anisotropy fields needed for fitting the linewidth data were determined by analyzing the angular dependence of FMR field as shown in Fig. 2. The fitting parameters Γ_0 and $\langle c/a \rangle$ of Eq. (12) both affect the vertical scale of ΔH vs ϕ_H, but $\langle c/a \rangle$ also affects the shape of the curve. Thus, by fitting the theory to the data, we can obtain information about the parameters related to the extrinsic two-magnon process. Taking into account only one of the mechanisms through to Eqs. (11), (12), or (13), one obtains the dashed curves. This shows that each of them separately is not sufficient to describe the magnetization relaxation of the films. The entire angular dependence of the FMR linewidth (solid line) can be explained by adding the two-magnon scattering and local inhomogeneous effects. In Fig. 3(b) we show the Gilbert (open circles) and the extrinsic ($\Delta H_{2M} + \Delta H^{mosaic}$, open squares) contributions to the linewidth for $t_{AF} \geqslant 54$ Å. In this region we can clearly identify both extrinsic and intrinsic processes. For lower values of t_{AF} the analysis of the data is not straightforward due to the fact that the angular variation of ΔH is less pronounced, and consequently in region I it remains undetermined which of the mechanisms is the most pronounced.

In order to get detailed information on the origin of the pronounced peak exhibited by the linewidth shown in Fig. 3(b), we decided to prepare a series of samples in which the different relaxation mechanisms could be extracted. Following this idea, we fabricate a series of $Ni_{81}Fe_{19}$(10 nm)/$Ir_{20}Mn_{80}$(t_{AF}) bilayers (named series B) by oblique sputtering at a deposition angle of 50°. It has been known that magnetic films fabricated under oblique deposition conditions can exhibit very strong uniaxial anisotropy (see Table II) that depends on the inclination angle of the substrate during the deposition process.[26] The origin of this growth-induced magnetic anisotropy has been attributed to columnar grain structures that grow tilted toward the deposition direction with respect to the substrate normal.[43–46] On the other hand, within the plane of the film, the self-shadowing effect that occurs during the film growth is more effective in the deposition flux direction, producing grains that tend to be elongated perpendicular to this direction.[47,48] These two effects, shape anisotropy and magnetocrystalline anisotropy, both contribute to the observed magnetic anisotropy of the films. As shown in Ref. 26 and emphasized here, the films grown by oblique sputter deposition turned out to be a useful prototype for the investigation of FM relaxation mechanisms.

The phenomenological parameters used in the calculation are $\gamma = 17.6$ GHz/kOe and $4\pi M_{eff} = 9.65$ kG, extracted from the fit of the experimental data corresponding to the $Ni_{81}Fe_{19}$ film grown under oblique angle conditions. The in-plane variations of the FMR fields for three samples of series B, shown in Fig. 5, exhibit a pronounced uniaxial anisotropy in comparison to the bilayers of series A, shown in Fig. 2.

TABLE I. Magnetic relaxation parameters extracted from the fit of the linewidth data. The samples were grown at a deposition angle of 0°.

t_{AF} (Å)	H_U (Oe)	α	ΔH_{2M} (Oe)	Γ_0 (Oe)	$\left\langle \frac{c}{a} \right\rangle$	ΔH_E (Oe)	$\Delta\beta$ (deg)	$\Delta\eta$ (deg)
61	40	0.006	43	37	1.003	12	11	0
80	45	0.006	39	34	1.002	16	13	0

TABLE II. Magnetic relaxation parameters extracted from the fit of the linewidth data showed in Fig. 7. All samples were grown at a deposition angle of 50°.

t_{AF} (Å)	H_U (Oe)	α	ΔH_{2M} (Oe)	Γ_0 (Oe)	$\left\langle \frac{c}{a} \right\rangle$	ΔH_E (Oe)	$\Delta\beta$ (deg)	$\Delta\eta$ (deg)
2	90	0.006	17	13	1.019	0	0	0
6	90	0.007	17	13	1.018	0	0	0
19	125	0.008	60	46	1.013	0	0	0
33	130	0.009	34	26	1.012	4	0	0
45	110	0.008	39	30	1.017	12	0	0
56	119	0.008	39	30	1.016	11	0	0

This is clear from the angular dependence of the resonance field that shows two peaks near $\phi_H = 90°$ and $\phi_H = 270°$. Furthermore, the curves at different AF thicknesses exhibit two different features. The average values of H_R are shifted along the vertical axis by an amount given by H_{RA} and the unidirectional symmetry becomes evident as t_{AF} increases. Figure 6(a) shows the exchange field H_E (circles) and the rotatable anisotropy field H_{RA} (squares) as a function of the AF layer thickness for all samples of series B. As can be seen, as the samples of series A, three regions are clearly distinguished: region I, in which the exchange field H_E is null and the H_{RA} value increases; region II, where EB starts to establish and H_{RA} reduces; and region III, where all the fields reach saturation. This shows that the same interplay between rotatable and frozen AF grains occurs in the samples grown at an oblique angle of 50°, as was investigated in the samples grown at an oblique angle of 0°.

The solid circles in Fig. 6 show the average values of the FMR linewidth as a function of the AF layer thickness for the samples of series B. As one can see, following the trend observed in the samples of series A [see Fig. 3], ΔH experiences a nonmonotonic behavior with increasing t_{AF}. First it exhibits a maximum at $t_{AF} = 17$ Å, and then it decreases until it reaches saturation at $t_{AF} = 20$ Å. Notice that this interval corresponds to region I of Fig. 6(a) in which H_{RA} attains its maximum value. As previously explained, at low values of t_{AF}, where the AF layers do not exhibit a stable AF ordering with fluctuations of its magnetization contributing to the enhancement of the magnetic damping, the origins of the relaxation mechanisms were not obvious. Actually, as is clear from the results shown in Fig. 6(b), the dominant contribution to the linewidth in this interval (17 Å $\leqslant$ t_{AF} $\leqslant$ 22 Å) is due to the two-magnon scattering mechanism. This supports our assumption that the onset of H_{RA} is related to the existence of unstable AF grains. Below $t_{AF} = 17$ Å, the two-magnon scattering and Gilbert relaxation processes are the two main operative mechanisms. For $t_{AF} > 22$ Å we have to also consider the contribution from mosaicity in addition to two-magnon scattering and Gilbert processes [see Eq. (10)].

The angular dependence of the linewidth for some representative bilayers of series B are shown in Fig. 7. As we mentioned, these films exhibit a high uniaxial anisotropy, and consequently the angular dependence of ΔH shows a pronounced uniaxial symmetry. This is a clear signature of the occurrence of the two-magnon scattering mechanism that

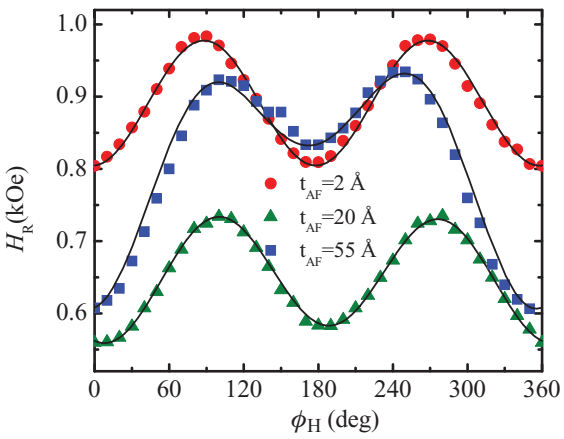

FIG. 5. (Color online) In-plane angular dependence of the FMR resonance field for bilayers with three different AF layer thicknesses (the solid lines are fit to the data). The FM-AF bilayers were grown at a deposition angle of 50°.

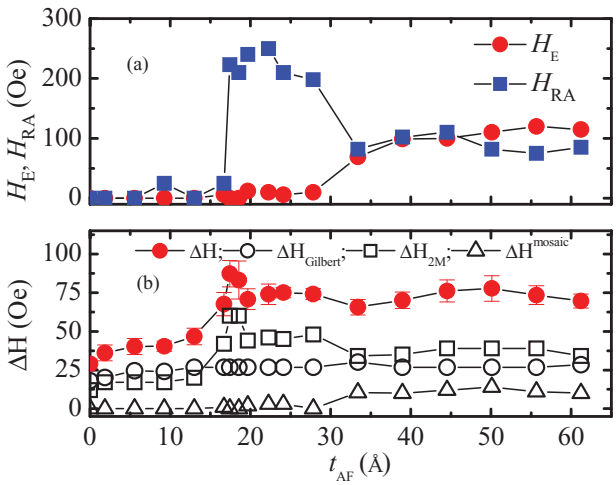

FIG. 6. (Color online) (a) AF layer thickness dependence of the EB field H_E (circles) and rotatable anisotropy field H_{RA} (squares) obtained from the fitting of the FMR data. (b) AF layer thickness dependence of the FMR linewidth (solid circles). The linewidth value is averaged over all the in-plane resonance spectra for each sample. The open symbols correspond to the intrinsic and extrinsic contributions to the linewidth. All the samples were grown at a deposition angle of 50°. The solid lines in (a) and (b) are a guide for the eye.

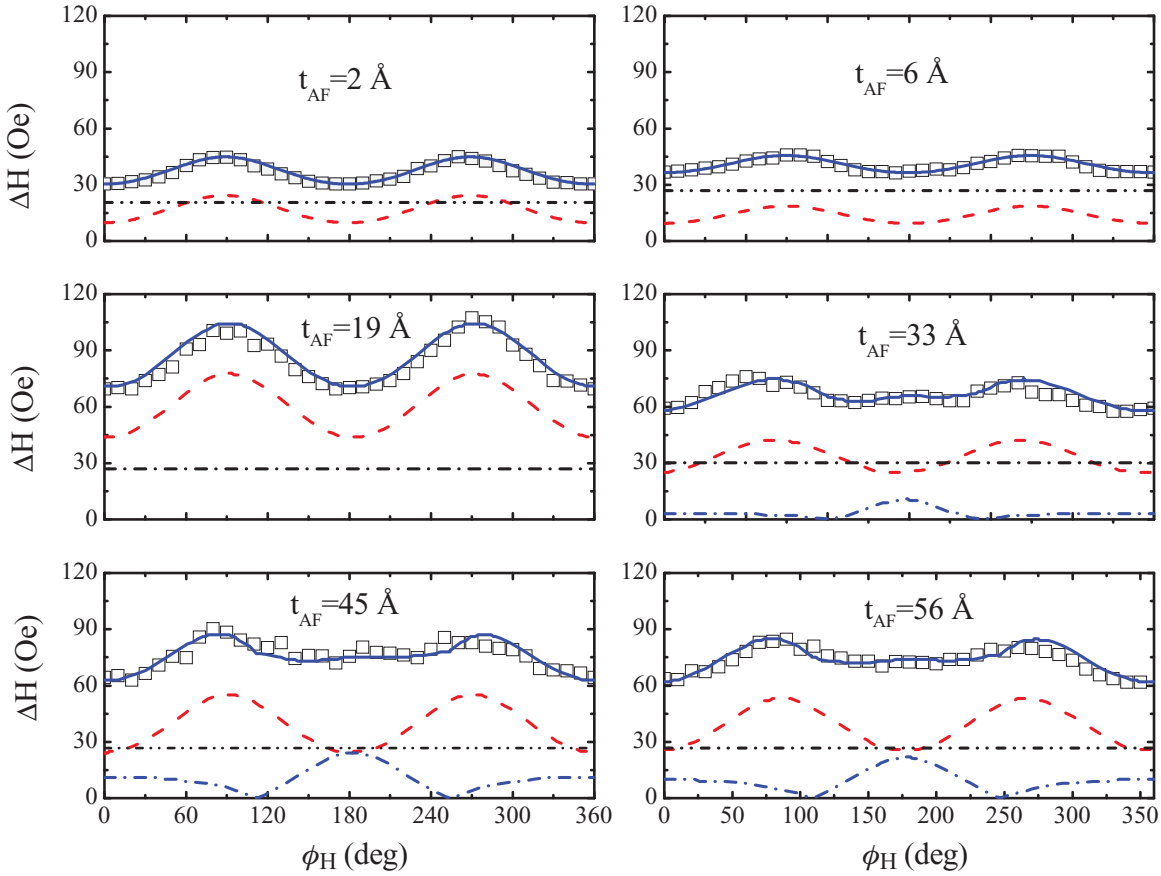

FIG. 7. (Color online) Angular dependence of the FMR linewidths for the bilayers deposited at an angle of 50°. The squares are the experimental data obtained at a frequency of 8.61 GHz, whereas the solid lines are fits obtained from Eq. (10) with the parameters showed in the Table II. The dashed lines correspond to the individual contributions of the three relaxation mechanisms considered (ΔH_{2M}: dashed line; ΔH^{mosaic}: dashed-dotted line; $\Delta H_{\text{Gilbert}}$: dashed-dotted-dotted line).

becomes quite active in these samples. The dashed curves in Fig. 7 represent the contributions of each of the three different relaxation mechanisms considered [see Eq. (13)]. As we can see, the presence of ΔH^{mosaic} due to the strong variation of H_E at the FM-AF interface (ΔH_E, see Table II), for $t_{\text{AF}} = 33$, 45, and 56 Å, tends to break the uniaxial symmetry coming from the ΔH_{2M} mechanism. The fits also reveal that the average spread of the direction of the easy axes in the FM and AF films (represented by $\Delta\eta$ and $\Delta\beta$, respectively) is negligible.

V. CONCLUSIONS

In summary, we have studied the AF thickness dependence of the exchange bias, the rotatable anisotropy field, and the FMR linewidth in polycrystalline $Ni_{81}Fe_{19}/Ir_{20}Mn_{80}$ bilayers. The different trends of the rotatable anisotropy and EB fields are correlated with the stability of the AF grains at the interface, confirming the assumption that the isotropic resonance field shift is induced by the rotatable anisotropy. We believe that this is a general feature of the EB polycrystalline systems. The FMR linewidth shows a nonmonotonic dependence on the AF thickness. We confirmed that the model of Arias and Mills[33] is capable of quantitatively describing the angular dependence of the measured linewidth. Besides, the Gilbert damping, the two-magnon damping, and the mosaicity effects strongly affect its dependence. We showed that the effective magnetic damping can be adjusted over a wide range by changing the AF thickness. In particular, we found that the peak in the FMR linewidth at certain AF thickness is due to the enhancement of the two-magnon scattering. These results are important for applications that require the understanding of how tune the magnetic damping, which is directly applied in the dynamic response in spintronic devices.

ACKNOWLEDGMENTS

This work has been supported by the Brazilian agencies CNPq, CAPES, FINEP, FACEPE, by the Fondo Nacional de Investigaciones Científicas y Tecnológicas (FONDECYT, Chile) under Grants No. 1085229 and No. 11080246, by Millennium Science Nucleus "Basic and Applied Magnetism" Grant N°P10-061-F, and by the Financiamiento Basal para Centros Científicos y Tecnológicos de Excelencia CEDENNA FB0807.

[1]W. H. Meiklejohn and C. P. Bean, Phys. Rev. **102**, 1413 (1956).
[2]J. Nogués and I. K. Schuller, J. Magn. Magn. Mater. **192**, 203 (1999).
[3]A. E. Berkowitz and K. Takano, J. Magn. Magn. Mater. **200**, 552 (1999).
[4]J. Nogués, J. Sort, V. Langlais, V. Skumryev, S. Suriñach, J. S. Muñoz and M. D. Baró, Phys. Rep. **422**, 65 (2005).
[5]R. L. Stamps, J. Phys. D **33**, R247 (2000).
[6]M. Kiwi, J. Magn. Magn. Mater. **234**, 584 (2001).
[7]F. Radu and H. Zabel, Springer Tracts Mod. Phys. **227**, 97 (2008).
[8]K. O'Grady, L. E. Fernandez-Outon, and G. Vallejo-Fernandez, J. Magn. Magn. Mater. **322**, 883 (2010).
[9]J. R. Fermin, M. A. Lucena, A. Azevedo, F. M. de Aguiar, and S. M. Rezende, J. Appl. Phys. **87**, 6421 (2000).
[10]R. L. Rodríguez-Suárez, L. H. Vilela-Leão, F. M. de Aguiar, and S. M. Rezende, J. Appl. Phys. **97**, 4544 (2003).
[11]L. Néel, Ann. Phys. **2**, 61 (1967); *English translation: Selected Works of Louis Néel*, edited by N. Kurti (Gordon & Breach, New York, 1988), p. 475.
[12]D. Mauri, H. C. Siegmann, P. S. Bagus, and E. Kay, J. Appl. Phys. **62**, 3047 (1987).
[13]M. D. Stiles and R. D. McMichael, Phys. Rev. B **59**, 3722 (1999).
[14]S. Polisetty, S. Sahoo, and C. Binek, Phys. Rev. B **76**, 184423 (2007).
[15]J. Geshev, S. Nicolodi, R. B. da Silva, J. Nogués, V. Skumryev, and M. D. Baró, J. Appl. Phys. **105**, 053903 (2009).
[16]J. Wu, J. S. Park, W. Kim, E. Arenholz, M. Liberati, A. Scholl, Y. Z. Wu, Chanyong Hwang, and Z. Q. Qiu, Phys. Rev. Lett. **104**, 217204 (2010).
[17]J. McCord, C. Hamann, R. Schäfer, L. Schultz, and R. Mattheis, Phys. Rev. B **78**, 094419 (2008).
[18]J. McCord, R. Mattheis, and D. Elefant, Phys. Rev. B **70**, 094420 (2004).
[19]J. McCord, R. Kaltofen, T. Gemming, R. Hühne, and L. Schultz, Phys. Rev. B **75**, 134418 (2007).
[20]S. K. Mishra, F. Radu, S. Valencia, D. Schmitz, E. Schierle, H. A. Dürr, and W. Eberhardt, Phys. Rev. B **81**, 212404 (2010).
[21]P. Y. Yang, C. Song, B. Fan, F. Zeng, and F. Pan, J. Appl. Phys. **106**, 013902 (2009).
[22]S. M. Rezende, M. A. Lucena, A. Azevedo, A. B. Oliveira, F. M. de Aguiar, and W. F. Egelhoff, Jr., J. Magn. Magn. Mater. **226**, 1683 (2001).
[23]J. R. Fermin, M. A. Lucena, A. Acevedo, F. M. de Aguiar, and S. M. Rezende, J. Appl. Phys. **87**, 6421 (2000).
[24]R. L. Rodríguez-Suárez, S. M. Rezende, and A. Azevedo, Phys. Rev. B **71**, 224406 (2005).
[25]R. L. Rodríguez-Suárez, A. B. Oliveira, S. M. Rezende, and A. Azevedo, J. Appl. Phys. **99**, 08R506 (2006).
[26]J. B. Santos Mendes, L. H. Vilela-Leão, S. M. Rezende, and A. Azevedo, IEEE Trans. Magn. **46**, 2293 (2010).
[27]*Collected Papers of L. D. Landau*, edited by D.Ter Haar, (Gordon & Breach, New York/Pergamon, Oxford, 1965), Chap. 18, p. 101.
[28]B. Heinrich, *Ultrathin Magnetic Structures III* (Springer, New York, 2004), Chap. 5, p. 143.
[29]J. Smit and H. G. Beljers, Philips Res. Rep. **10**, 113 (1955).
[30]J. Geshev, L. G. Pereira, and J. E. Schmidt, Phys. Rev. B **64**, 184411 (2001).
[31]S. V. Vonsovskii, *Ferromagnetic Resonance* (Pergamon, Oxford, UK, 1966).
[32]D. L. Mills and S. M. Rezende, Top. Appl. Phys. **87**, 27 (2003).
[33]R. Arias and D. L. Mills, Phys. Rev. B **60**, 7395 (1999).
[34]A. Azevedo, A. B. Oliveira, F. M. de Aguiar, and S. M. Rezende, Phys. Rev. B **62**, 5331 (2000).
[35]S. M. Rezende, A. Azevedo, M. A. Lucena, and F. M. de Aguiar, Phys. Rev. B **63**, 214418 (2001).
[36]G. Woltersdorf and B. Heinrich, Phys. Rev. B **69**, 184417 (2004).
[37]K. Zakeri, J. Lindner, I. Barsukov, R. Meckenstock, M. Farle, U. von Hörsten, H. Wende, W. Keune, J. Rocker, S. S. Kalarickal, K. Lenz, W. Kuch, K. Baberschke, and Z. Frait, Phys. Rev. B **76**, 104416 (2007).
[38]P. Landeros, R. E. Arias, and D. L. Mills, Phys. Rev. B **77**, 214405 (2008).
[39]J. Lindner, I. Barsukov, C. Raeder, C. Hassel, O. Posth, R. Meckenstock, P. Landeros, and D. L. Mills, Phys. Rev B **80**, 224421 (2009).
[40]P. Landeros, J. Lindner, R. E. Arias, and D. L. Mills (unpublished).
[41]R. D. McMichael, D. J. Twisselmann, and A. Kunz, Phys. Rev. Lett. **90**, 227601 (2003).
[42]J. R. Fermin, A. Azevedo, F. M. de Aguiar, B. Li, and S. M. Rezende, J. Appl. Phys. **85**, 7316 (1999).
[43]D. O. Smith, J. Appl. Phys. **87**, 264S (1959).
[44]S. van Dijken, G. Di Santo, and B. Poelsema, Appl. Phys. Lett. **77**, 2030 (2000).
[45]R. D. McMichael, C. G. Lee, J. E. Bonevich, P. J. Chen, W. Miller, and W. F. Egelhoff Jr., J. Appl. Phys. **88**, 3561 (2000).
[46]M. T. Umlor, Appl. Phys. Lett. **87**, 082505 (2005).
[47]H. Konig and G. Helwig, Optik (Stuttgart) **6**, 111 (1950).
[48]Y. Hoshi, E. Suzuki, and M. Naoe, J. Appl. Phys. **79**, 4945 (1996).